Journal of Electroanalytical Chemistry 840 (2019) 367–375

Contents lists available at ScienceDirect

Journal of Electroanalytical Chemistry

journal homepage: www.elsevier.com/locate/jelechem

Investigation of the electrocatalytic activity for ethanol oxidation of Pt nanoparticles modified with small amount (≤ 5 wt%) of CeO_2

Maria J. Paulo[a], Ricardo H.D. Venancio[c], Renato G. Freitas[b,c], Ernesto C. Pereira[b], Ana C. Tavares[a,*]

[a] Institut National de la Recherche Scientifique — Énergie, Matériaux et Télécommunications, 1650 Boulevard Lionel-Boulet, Varennes, Québec J3X 1S2, Canada
[b] Laboratório Interdisciplinar de Eletroquímica e Cerâmica, Centro Multidisciplinar para o Desenvolvimento de Materiais Cerâmicos, Departamento de Química, Universidade Federal de São Carlos, C.P.: 676, CEP 13565-905 São Carlos, SP, Brazil
[c] Laboratório Computacional de Materiais, Departamento de Química, Universidade Federal de Mato Grosso, Cuiaba CEP: 78060-900, MT, Brazil

ARTICLE INFO

Keywords:
Ethanol oxidation
Platinum nanoparticles
Ceria nanoparticles
Electronic interaction
Microstrain

ABSTRACT

Pt is still the state of the art electrocatalyst for the oxidation of ethanol but it is poisoned by the CO-intermediates resulting in a slow ethanol oxidation reaction kinetic. Here, we show that the electrocatalytic activity of unsupported Pt nanoparticles for the ethanol electro-oxidation in acid medium can be significantly enhanced by the addition of small amounts of CeO_2 nanoparticles (≤ 5 wt%). Comparative studies on bare Pt, Pt-$CeO_2$1 wt% and Pt-CeO_2—5 wt% catalysts composed of Pt nanoparticles with different sizes (from 10 to > 40 nm for bare Pt, and from 6 and 20 nm for the Pt-CeO_2 composites) revealed an increase of the microstrain with the decrease of the Pt's average particle size. Besides, there is a strong electronic interaction between the Pt and CeO_2 nanoparticles, demonstrated by a systematic shift of the Pt $4f_{7/2}$ peak to lower binding energy with the addition of CeO_2. Chronoamperometric data showed that the steady state current density normalized to Pt's electrochemical surface area for ethanol electro-oxidation is mainly governed by the microstrain, and it decreases with increasing strain. This trend is explained in terms of a more facile activation of the ethanol molecule at the surface of less strained Pt nanoparticles. Thus, the best performance was obtained with Pt-CeO_2 1 wt% formed by Pt nanoparticles with an average size of 18 nm, reaching 1.0 $A{\cdot}m^{-2}$ after 900 s at 0.6 V vs SCE.

1. Introduction

Methanol and ethanol are liquid fuels with very high energy density (6.09 kWh kg^{-1} for methanol and 8.01 kWh kg^{-1} for ethanol) and are easy to handle. These fuels and hydrogen produced in a sustainable way constitute alternatives to fossil fuels. Ethanol is safer (lower toxicity) than methanol, and it is a green fuel produced by the fermentation of sugar-raw materials [1–3]. However, the successful application of the ethanol fuel cell technology, depends on the availability of a catalyst that is capable of breaking the C—C bond leading to CO_2 as the final product, instead of intermediates as acetic acid, acetaldehyde and adsorbed CO-like species [4]. Platinum is still the most efficient electrocatalyst for the oxidation of ethanol in acid medium, in terms of cleavage of the C—C bond [5,6]. Still, it is poisoned by the CO-intermediates resulting in a slow ethanol oxidation reaction kinetic [6,7]. To circumvent this problem a second element such as Ru and Sn, or even a third one as Ni, Ir and Os, have been added to Pt nanoparticles as co-catalysts [8,9]. The synergistic effect of the second metal is generally explained by two processes: electronic destabilization of the Pt-CO bond, weakening its strength allowing a facile CO electro-oxidation to CO_2; or by the bifunctional effect where the second element is oxophilic (i.e., it is present as M-OH or M-H_2O), bringing the necessary oxygen to the Pt neighboring site favoring the oxidative removal of CO-like species [8,10,11].

The addition of metal oxides such as RuO_2 [9], WO_3 [12], ZrO_2 [13], TiO_2 [14] and CeO_2 [7,15,16] have also been found to enhance the catalytic activity of Pt for ethanol or methanol electro-oxidation through synergetic interaction. In fact, noble metal–cerium dioxide composite catalysts are among the systems known to exhibit strong catalyst and co-catalyst interactions in heterogeneous catalysis [17–19]. For example, the partial oxidation of methanol to formaldehyde and formic acid is strongly promoted by Pt partially covered by CeO_2 [17], and the oxidation of CO on Pt(111) encapsulated by CeO_2 [19]. Similar findings were found for the methanol and ethanol electro-oxidation in acid environment [20–23]. Gu et al. [20] investigated the methanol electro-oxidation on Pt-CeO_2/C catalysts prepared by

* Corresponding author.
E-mail address: ana.tavares@emt.inrs.ca (A.C. Tavares).

https://doi.org/10.1016/j.jelechem.2019.04.008
Received 24 September 2018; Received in revised form 3 March 2019; Accepted 1 April 2019
Available online 02 April 2019
1572-6657/

microwave-assisted method with mass contents of CeO_2 from 10 to 60 wt%, and a constant loading of Pt of 20 wt%. The catalyst with highest electrocatalytic activity and stability for the oxidation of both alcohols contains 20 wt% CeO_2, and it was explained in terms of promotion of the oxidation of CO_{ads} species, better dispersion of the Pt nanoparticles (NPs) induced by the oxide, and a good stability of the CeO_2–C support in acidic media. Yang et al. [24] combined the reduction and sol-gel methods to produce a series of CeO_2-Pt nanorods/C nanoparticles, finding out that the catalyst with 35 wt% CeO_2-Pt/C has the highest current for methanol oxidation reaction. The authors suggested that the positive influence of CeO_2 on the platinum activity is due to bifunctional mechanism. In another work, Scibioh et al. [21] investigated the methanol oxidation on 40 wt% Pt-CeO_2/C catalysts. First, the substrate (3–12 wt%) CeO_2 supported onto carbon was prepared, followed by the deposition of 40 wt% of Pt by wet impregnation method and reduction with H_2. The authors reported that 9.0 wt% of ceria is enough to increase the activity of the catalyst of about 50% compared to the Pt/C catalyst. CO-stripping measurements showed a more facile removal of intermediate poisoning species in the presence of the oxide, and both bifunctional and electronic mechanisms were proposed. In another work, Yu et al. [16] investigated the effect of 20 wt% of ceria on Pt/C on the electro-oxidation of several alcohols in acid medium, obtaining higher electro-oxidation currents than for pure Pt. For all tested small organic molecules, an increase of 35% for methanol, 64% for ethanol, 87% for ethylene glycol, and 82% for glycerol, was achieved respectively. The authors explained this increase in terms of bifunctional effect. Similar trends were found for the oxidation of the same small organic molecules in alkaline media using a Pt–CeO_2 (1:1 by weight)/C catalyst [25]. De Souza et al. [22] studied Pt-CeO_2/C (20 wt % of Pt-CeO_2 on carbon XC-72R; and Pt:Ce mass ratio of 3:1, 2:1, 1:1, 1:2, 1:3) prepared by the polymeric precursor method for the ethanol electro-oxidation. Once again, it was verified that the presence of CeO_2 promotes the rate of the alcohol oxidation, but the highest intrinsic activity (in $mA{\cdot}mg^{-1}$) was observed for the catalyst with 75 wt% CeO_2 and the lowest activity for the catalyst with 50 wt% CeO_2. This unusual trend was related with the maximum utilization of the Pt surface. It was found that catalysts with lower Pt (higher CeO_2) content have the lowest mean Pt crystallite size (~4 nm), and thus the highest electrochemical surface area.

There is no consensus in the literature on the amount of ceria that should be added to Pt in order to maximize its catalytic activity towards methanol and ethanol electro-oxidation. This is probably due to the different compositions investigated (Pt:CeO_2 mass ratio) as well as different synthetic methods used to prepare the catalysts which have a marked effect on their properties. On one hand, CeO_2 can prevent the growth and sintering of Pt nanoparticles. On the other hand, the ratio Ce^{4+} to Ce^{3+} can be dependent on the CeO_2 preparation method, particle size and aging of the CeO_2 nanoparticles [15,25,26]. For instance, high temperature synthesis produce larger CeO_2 nanoparticles with a higher amount of surface Ce^{4+} species than the lower temperature methods [26,27]. In fact, the bifunctional mechanism postulated to justify the enhancement of the oxidation of methanol and ethanol in acid and in alkaline media [25,28] puts in evidence the oxygen donor capability of CeO_2 and the importance of Ce^{4+} ions in the reaction:

$$Pt\text{-}CO_{ads} + 4\ CeO_2 + 2H^+ + 2e^- \rightarrow 2\ Ce_2O_3 + Pt + CO_2 + H_2O \quad (1)$$

This work investigates the ethanol electro-oxidation on Pt-CeO_2 composite catalysts with oxide content up to 5 wt% with respect to the Pt mass. To the best of our knowledge there is a gap of studies on the electrocatalytic activity of composites containing small amounts of this semiconductor oxide. As in the “inverse supported catalyst”, where a semiconductor is supported on a metallic substrate [17], electronic effects on these catalysts could be very large because the number of free electrons in the metal is several orders of magnitude higher than that of the semiconductor [29]. Besides, very small amounts of CeO_2 can lead to important strain of the Pt lattice during particle growth which could change the surface free energy of the system.

The Pt and Pt-CeO_2 catalysts were synthesized using the Pechini method [30] a straightforward method for the synthesis of Pt nanoparticles in one single step [31]. As it will be shown, it provides a very good degree of flexibility in the preparation of catalysts, and the possibility of investigating the CeO_2/Pt interaction for a wide range of Pt particle sizes (from ca. 40 nm down to 4 nm). Three series of Pt-CeO_2 catalysts with 0, 1 and 5 wt% CeO_2 were prepared and tested for the ethanol electro-oxidation in acidic media. No carbon, or any other substrate, was used to support the nanoparticles, in order to rule out any effect coming from the carbon substrate. The influence of the catalysts' microstructure, particle size, surface composition and shifts in the binding energy of Pt 4f and Ce 3d XPS peaks on the electrocatalytic activity of the Pt-CeO_2 catalysts are discussed.

2. Experimental

2.1. Materials

Hexachloroplatinic acid ($H_2PtCl_6{\cdot}6H_2O$, 99.9%, Alfa Aesar), citric acid ($Na_3C_6H_5O_7$, 99%, Fisher Scientific), ethanol (anhydrous, Commercial Alcohols), ethylene glycol ($C_2H_6O_2$, from Sigma Aldrich), sulfuric acid (from Sigma Aldrich (95–98%) and ammonium cerium (IV) nitrate ($(NH_4)_2Ce(NO_3)_6$, 98.5%, Acros Organics) were used as received. MiliQ water was used throughout the investigation.

2.2. Synthesis of Pt and Pt-CeO_2 nanoparticles

Platinum nanoparticles were prepared by first dissolving citric acid (CA) in ethylene glycol (EG) at 60 °C followed by the addition of H_2PtCl_6 to the solution. This precursor solution was first jellified at 130 °C for 30 min and a high molecular weight polymer was obtained through successive esterification reactions [32]. The gel was then pyrolyzed at 400 °C for 4 h resulting in the formation of the Pt NPs. Three series of catalysts were prepared from precursors containing different amounts (successive dilution) of Pt precursor salt in the CA-EG polymer gel. In the first series, identified as 1×, the Pt:CA:EG molar ratio was 1:12:96; in the second series, identified as 5×, the molar ratio was 0.2:12:96; and in the third series, identified as 10×, the molar ratio was 0.1:12:96. For the bimetallic catalysts, a stoichiometric amount of $(NH_4)_2Ce(NO_3)_6$ was also added to the reaction mixture at 60 °C. Two compositions were prepared, 1 and 5 wt% of CeO_2 with respect to Pt mass. These catalysts are referred as Pt-CeO_2 1 wt% and Pt-CeO_2 5 wt%.

2.3. Physicochemical characterization of the electrocatalysts

The phase composition and crystal structure of the catalysts was verified on a Bruker AXDS8 instrument with a Cu K_α radiation (λ = 1.54184 Å) operating at 40 mV and 40 mA. The diffractograms were collected in the 2θ range between 30° and 90° with a step of 0.05° and a measuring time of 5 s per point. The microstructural data of Pt and Pt-CeO_2 catalysts were obtained by the Rietveld refinement [33] using the General Structure Analysis System (GSAS) program [34] suite with the EXPGUI interface [35]. The original Rietveld formulation and many of its successors [36] treat the diffraction line width as a smooth function of the *d*-spacing of the diffraction angle (2θ), whereas many peaks of interest near 2θ have very different widths. Hence, in this work, the peak profile function developed by Stephens et al. [37] was used to fit the experimental data. In this method, it is considered that the diffraction peaks widths are not a smooth function of *d*, meaning that they might arise from anisotropic broadening of the crystallite size or from a particular pattern of defects (e.g. stacking faults). Finally, the bi-dimensional model for the crystallite size described by Larson and von Dreele [34] was used to account for the crystallite anisotropy.

The morphology and microstructure of the Pt and Pt-CeO_2 composites were investigated by transmission electron microscopy (TEM). Transmission electron micrographs were obtained with a JEOL 2100F operated at 200 kV (Center for Characterization of Microscopic Materials, at Ecole Polytechnique de Montreal). The TEM samples were prepared by dipping the copper grids on the powder samples already dispersed in methanol. The software ImageJ was used for the particle size statistics.

The X-ray photo-electron spectra were recorded using a VG Escalab 220i-XL using Al-Kα polychromatic radiation (hυ = 1487 eV) operating at 15 kV and 26.6 mA. The signal was filtered with a hemispherical analyzer (pass energy = 20 eV for the high resolution scans) and the detection was performed with a multi-channel detector. The main chamber pressure was kept $\leq 10^{-9}$ Torr during measurements. Particular care was exercised for the CeO_2 containing samples to minimize the reduction of Ce (IV) to Ce (III). Each sample was introduced in the chamber just before the analysis and the Ce (3d) spectrum was recorded just after the survey spectrum and in the end of the analysis. The binding energy of the spectra was calibrated with respect to the Carbon 1s peak at 284.5 eV. The core level spectra were peak-fitted using Lorentzian and Gaussian curves after the Shirley type background subtraction, and Casa XPS software. Peak areas were normalized by appropriate atomic sensitivity factors.

2.4. Electrodes preparation and electrochemical characterization

Electrochemical measurements were carried out in a three-electrode cell by using an Autolab potentiostat/galvanostat PGSTAT 302 N equipped with the SCANGEN module. A platinum wire and a leak less Saturated Calomel Electrode (SCE) were used as counter and reference electrodes, respectively. The working electrode is a glassy carbon disk electrode (Metrohm, 0.196 cm^2 geometric area) previously polished with Al_2O_3 paste and washed in distilled water followed by deposition of 5 μL of the catalyst ink. For the preparation of the catalyst ink, 2.5 mg of catalyst was weighted and diluted with 125 μL of ethanol and 25 μL of Nafion® suspension. This ink was sonicated for around 30 min. A 5 μL drop was micropipeted to the electrode surface and allowed to dry in air (room temperature) for 20 min. The mass of catalyst deposited on the Pt or Pt-CeO_2 electrodes is 0.083 mg which corresponds to a catalyst loading of 0.424 mg cm^{-2}. A high loading was necessary to form uniform catalyst layers on the glassy carbon electrode.

Cyclic voltammetry measurements were done in a 0.5 M H_2SO_4 electrolyte solution, previously purged with nitrogen for 20 min, in the −0.2 to 1.2 V vs SCE potential range first at 100 mV s^{-1} and after at 50 mV s^{-1}. Subsequently, the ethanol electro-oxidation was performed in a 1.0 M ethanol in 0.5 M H_2SO_4 solution. Cyclic voltammograms were recorded in the same potential range and data from the 10th cycle is reported. The chronoamperometry tests were performed right after cyclic voltammetry. The electrodes were first stabilized at −0.2 V vs SCE for 30 s, after which the potential of 0.6 V vs SCE was applied 900 s.

3. Results and discussion

The formation of metallic platinum with cubic *fcc* structure (JCPDS 04–0802) is confirmed in the X-ray diffractograms of the Pt and Pt-CeO_2 samples, Figs. S1 to S3. No diffraction peaks related to CeO_2 (JCPDS 34-0394) phase are observed in the diffractograms most probably due to the low ceria concentration in the Pt-CeO_2 samples. However, transmission electron microscopy combined with high resolution EDS analysis (Fig. S4) confirmed the presence of CeO_2 in the samples. Rietveld refinement of the diffractograms (Figs. S1 to S3) was used to calculate the lattice cell constant *a* and the microstrain of the Pt nanoparticles. As illustrated in Fig. 1a, *a* decreases with the increase of the dilution of the precursors in the gel and this could be due to a decrease of Pt's average particle size (see below for TEM analysis) [38,39]. The lattice constant

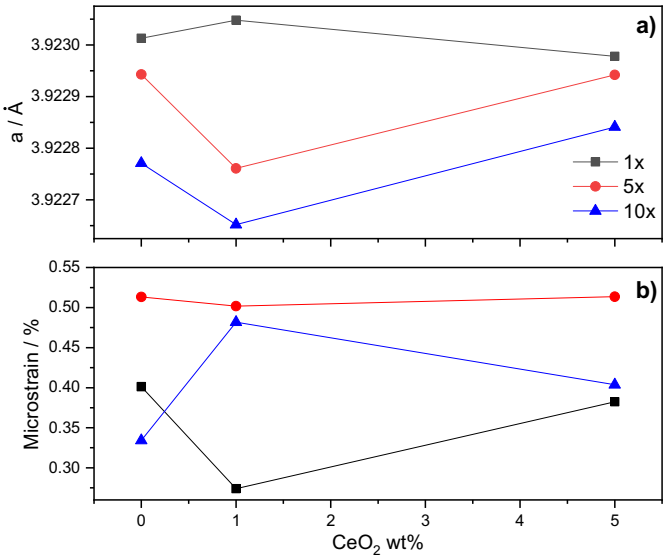

Fig. 1. Variation of (a) lattice cell parameter *a* and (b) microstrain as function of the ceria wt%. The dilution of the Pt and Ce precursors in the polyester gel are indicated in the figure.

is almost invariant for Pt and Pt-CeO_2 5 wt%, but interestingly it increases for Pt-CeO_2 1 wt% 1× and it decreases for Pt-CeO_2 1 wt% 5× and 10×, Fig. 1a. The microstrain also varies with the dilution of precursors in the polyester matrix, Fig. 1b. Again, for each series of dilution, there is an inflexion point at 1 wt% CeO_2. A correlation between the microstrain and Pt's average particle size is demonstrated next.

As shown in Fig. 2, Pt 1× sample is formed by nanoparticles with sizes ≥40 nm agglomerated in large clusters. As expected, the samples obtained from the diluted Pt precursor in the polyester polymeric network (Pt 5× and 10×) are formed by smaller (sizes < 40 nm) and less agglomerated nanoparticles. In these cases, the presence of partially burned carbon residues could also inhibit the grain growth. The mean particle size decreases from approximately 42 nm for the sample 1×, to 19.6 ± 6.5 and 15.2 ± 1.2 nm for 5× and 10× samples, respectively. It is interesting to note that Pt 10× shows a "mirroring-type" of growth where the planes are seeded together out of the plane (see inset in Fig. 2c). The presence of CeO_2, even in very small amounts, also promotes the decrease of the size and the deaglomeration of the Pt nanoparticles as evidenced in Fig. 2d and g. Individual Pt NPs with ca. 20 nm and 12 nm sizes can now be easily identified in samples Pt-CeO_2 1× with 1 and 5 wt% CeO_2 respectively. These Pt NPs are dispersed in a CeO_2 "matrix". However, the dilution of the Pt and Ce precursors in polyester polymer matrix revealed to be the most effective way to obtain samples mostly composed of well dispersed and small Pt NPs. A marked decrease of the particle size from 19.6 ± 6.5 nm for Pt-CeO_2-1 wt% to 4.3 ± 0.8 nm and 6.4 ± 1.7 nm for the 5× and 10× dilutions, respectively, is indeed observed (Fig. 2d and e). Samples Pt-CeO_2 5 wt% 5× and 10× are composed by Pt NPs with sizes slightly higher and with a broader size distribution than in Pt-CeO_2 1 wt% 5× and 10× (Fig. 2g). Because the Pt-CeO_2 1 wt% 10× also shows some particles with the "mirroring-type" of growth, this phenomenon seems to be caused by a dilution effect on Pt nanoparticles and not due to ceria since the mirroring is no longer visible in Pt-CeO_2 5 wt% 10×.

Synthesis of CeO_2 powders from gels with 1×, 5× and 10× dilutions, revealed the formation of NPs with average particle sizes between 6 and 8 nm, Fig. S5. Ceria is an oxidizing agent known to aid the combustion process lowering the temperature of oxidation of carbon [40]. Thus, the in-situ grown CeO_2 may accelerate locally the calcination process and facilitate the formation of smaller Pt nuclei [41]. Finally, as shown in Fig. 3, the expected inverse relationship between

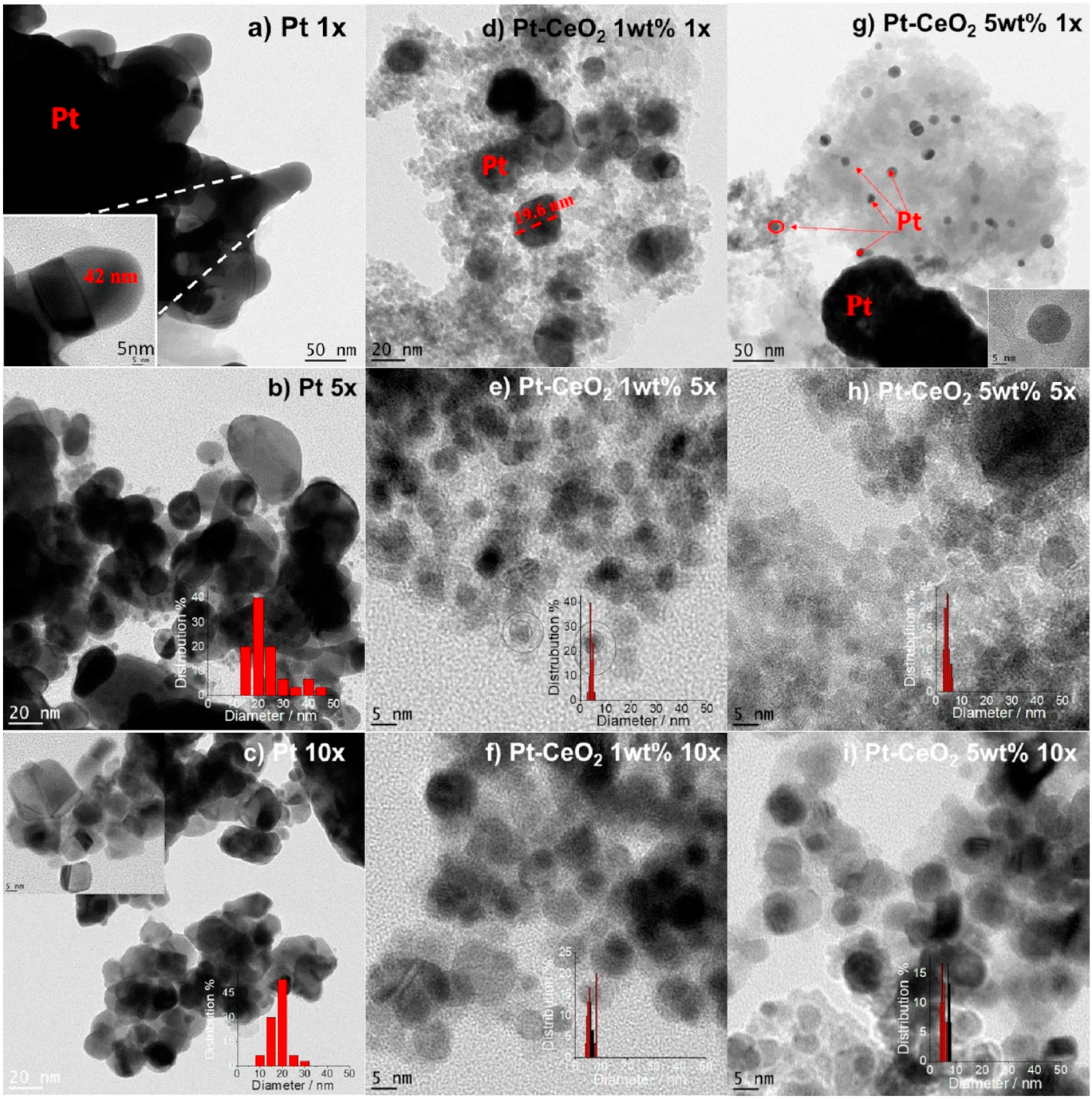

Fig. 2. TEM images of Pt (a) to (c), Pt-CeO_2 1 wt% (d) to (f) and Pt-CeO_2 5 wt% (g) to (i) nanoparticles. The statistics for the particle size distribution was done counting at least 200 particles on images with a 20 and 50 nm scale.

microstrain and average particle size [42] is observed for most of the catalysts. The two exceptions are Pt 1 × and Pt 5 × which are formed by agglomerated nanoparticles, and are less homogeneous in terms of particle size distribution.

X-ray photoelectron spectroscopy (XPS) is a technique that probes the surface composition and changes in an atom's core level structure, and was used to investigate catalysts. Fig. S6 shows the Pt 4f high resolution spectra for all Pt and Pt-CeO_2 catalysts under investigation. The two doublets of Pt 4f, namely $Pt4f_{7/2}$ and $Pt4f_{5/2}$ represent the two degenerated states of Pt separated by 3.33 eV and with an intensity ratio $Pt4f_{7/2}$:$Pt4f_{5/2}$ = 4/3. The Pt $4f_{7/2}$ peak around 71 eV corresponds to zero-valent Pt^0, while the very low intensity peak at higher binding energy i.e. 72.4 eV is assigned to Pt^{2+} [43]. It is well known that transition metal nanoparticles exhibit binding energy variations not only with its particle size but also with the chemical environment [44]. As observed in Fig. 4 all three series show a negative shift of $Pt4f_{7/2}$ binding energy with the addition of ceria. Initial state effects caused by a strong interaction between ceria and platinum are the most probable explanation. Negative shifts of Pt BE values were previously observed in Pt/Ni and Pt/Ru/Ni [45], Pt/Ru catalysts [46] and Pt/Sn [47] and were attributed to electron transfer from Ru (Ni or Sn) to Pt due to differences in the electronegativity between the two metals. There is also a considerable difference in electronegativity between Pt (2.28) and Ce (1.12), thus an electron transfer between the two elements is an appealing argument. In spite of the inflexion point at 1 wt% CeO_2 on the variation of *a* with the oxide content, we do not have solid any evidence

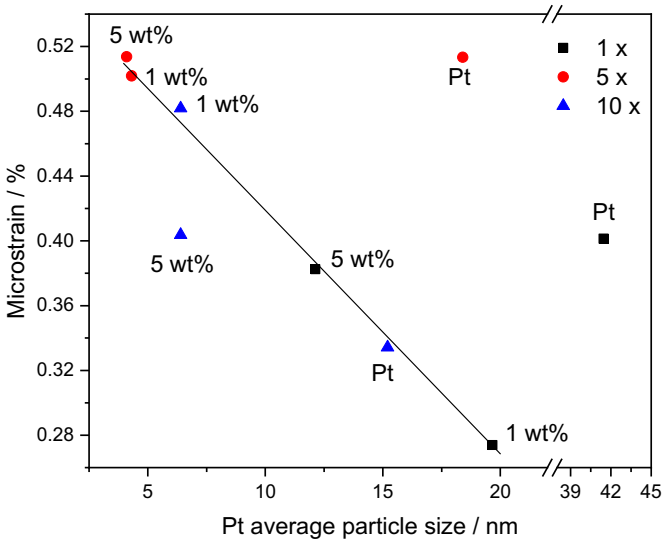

Fig. 3. Pt's microstrain as function of the nanoparticles' average particle size. The ceria wt% and of the dilution of the Pt and Ce precursors in the polyester gel are indicated in the figure.

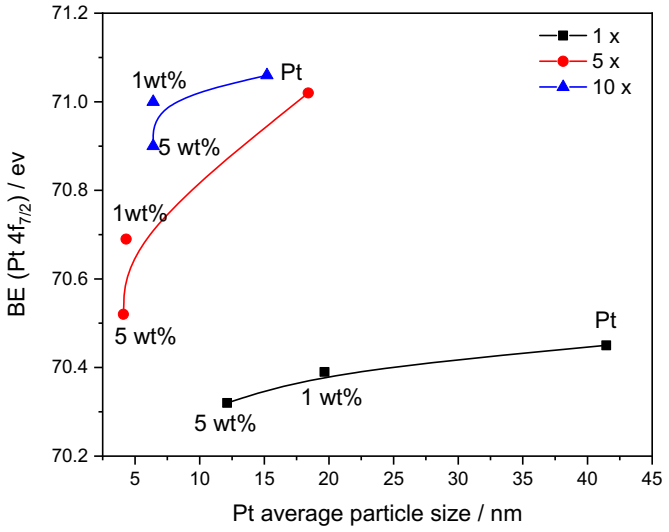

Fig. 4. Binding energy of Pt $4f_{7/2}$ as function of Pt nanoparticles' average particle size. The ceria wt% and of the dilution of the Pt and Ce precursors in the polyester gel are indicated in the figure.

of a formation of a Pt—Ce alloy or a Pt—Ce—O solid solution. Still, strong Pt–CeO_2 interactions via Pt—O—Ce bond have been reported before for Pt nanoparticles dispersed on nanosized ceria [48,49].

The effect of dilution produces an opposite trend with respect to that of the addition of ceria, and positive shifts are observed in the values of the binding energy of Pt $4f_{7/2}$. This shift is especially relevant for pure platinum 1× and 5× (0.6 eV positive shift) where the largest variation of particle size is observed, thus it could be related to a particle size effect by means of relaxation or core hole screening [50–52]. A $e^2/2r$ relationship between the binding energy and particle radius (e is the electron charge) has been established [52]. However, this effect is more pronounced on nanoparticles with diameters below 5 nm [53]. Thus, the positive shift may be related to a different structural arrangement of the Pt atoms on the particles' surface [51].

The Ce 3d core level spectra recorded for the Pt-CeO_2 composites and for pure CeO_2 (used as a reference to better understand the interaction between Pt and CeO_2 nanoparticles) are shown in Fig. S7. The spectra include two main cerium-rich bands that correspond to the $3d_{5/2}$ and $3d_{3/2}$ spin-orbit states. Moreover, the presence of mixed oxidation states results in a complex Ce 3d spectrum although Ce (III) can be differentiated from Ce (IV) due to different line shapes [54,55]. Namely, the v_2/v_2' and u_1/u_1' doublets, each separated by 18.6 eV, are assigned to the primary photoemission from Ce (IV) and Ce (III), respectively [56]. Detailed description of the spectra is reported in the Supporting Information section.

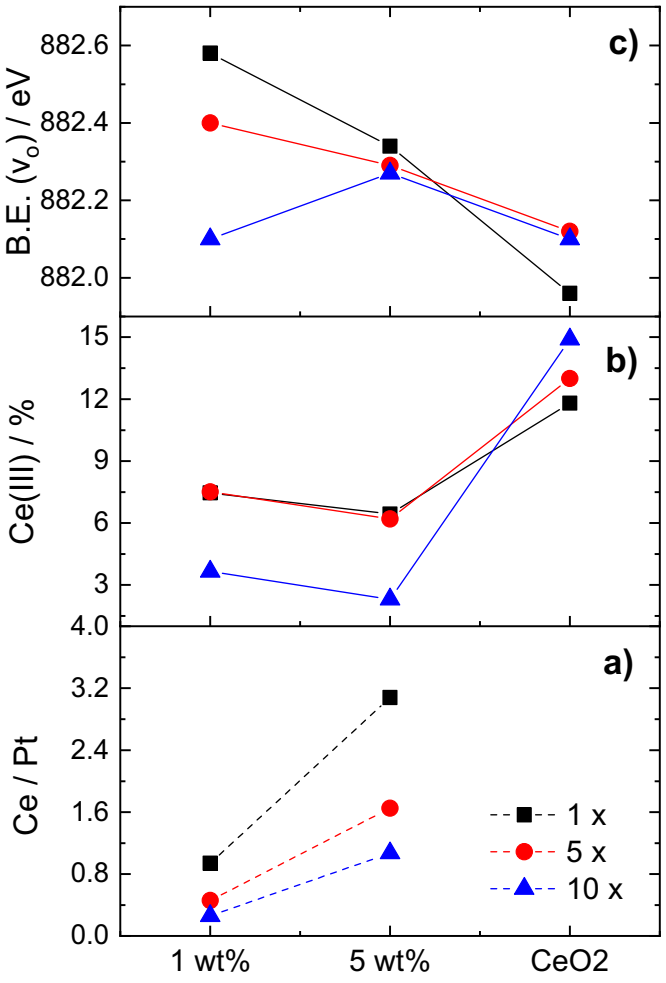

Fig. 5. (a) Ce/Pt at.% ratio, (b) % Ce (III) and (c) binding energy associated to v_0 (Ce(IV) main peak) in the Pt-CeO_2 catalysts and in CeO_2.

The surface Ce/Pt atomic ratio was calculated using the at.% obtained from the area under the peaks indicated in Eq. (2):

$$\frac{Ce}{Pt} = \frac{v_0 + u_1 + v_1 + v_2 + v_0' + u_1' + v_1' + v_2'}{(Pt\ 4f_{7/2})} \times 100 \quad (2)$$

As shown in Fig. 5a, the surface Ce/Pt atomic ratios are above 0.4 which is significantly higher than the nominal values of 0.01 for Pt-CeO_2 1 wt% and 0.06 for Pt-CeO_2 5 wt%. This is consistent with the TEM images presented in Fig. 2 that show the Pt NPs covered by CeO_2 NPs. As expected, the catalysts with higher amount of ceria, i.e. with 5 wt%, show the highest Ce/Pt ratio. The composites from series 1× have the highest Ce/Pt ratio which according to the TEM analysis can be explained by the agglomeration of the Pt NPs. XPS analysis also revealed that most of the surface cerium species are present as Ce (IV), Fig. 5b, which is consistent with the relatively high temperature used in the synthesis (400 °C) and small particle size of the CeO_2 nanoparticles [16].

The %Ce (III), was determined using the at.% obtained from the area under the peaks indicated in Eq. (3):

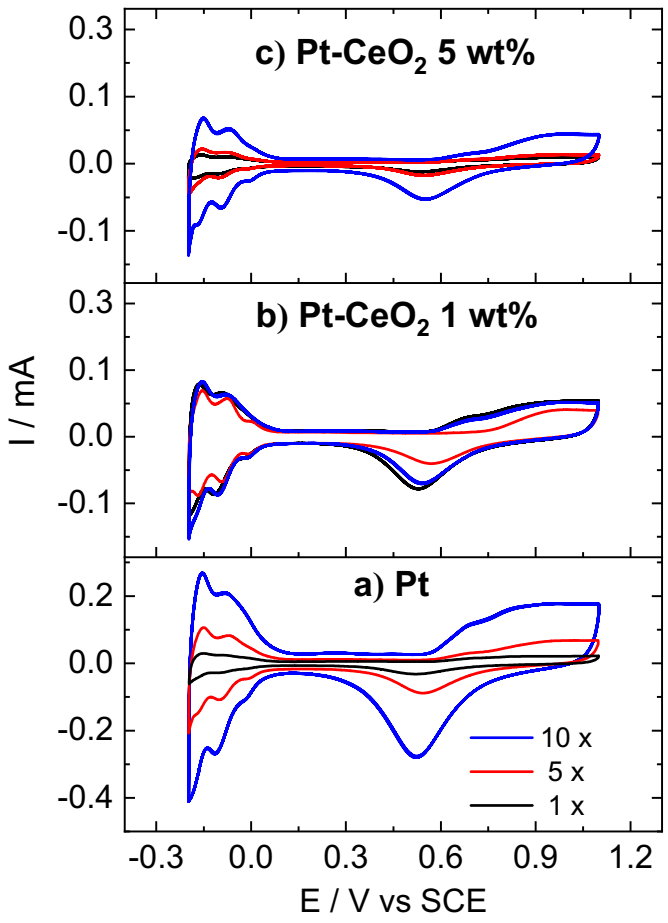

Fig. 6. Cyclic voltammograms in the 0.5 M H_2SO_4 electrolyte at 50 $mV{\cdot}s^{-1}$ for (a) Pt, (b) Pt-CeO_2 1 wt% and (c) Pt-CeO_2 5 wt% composites prepared with 1× (black), 5× (red) and 10× (blue) dilution in the polyester gel.

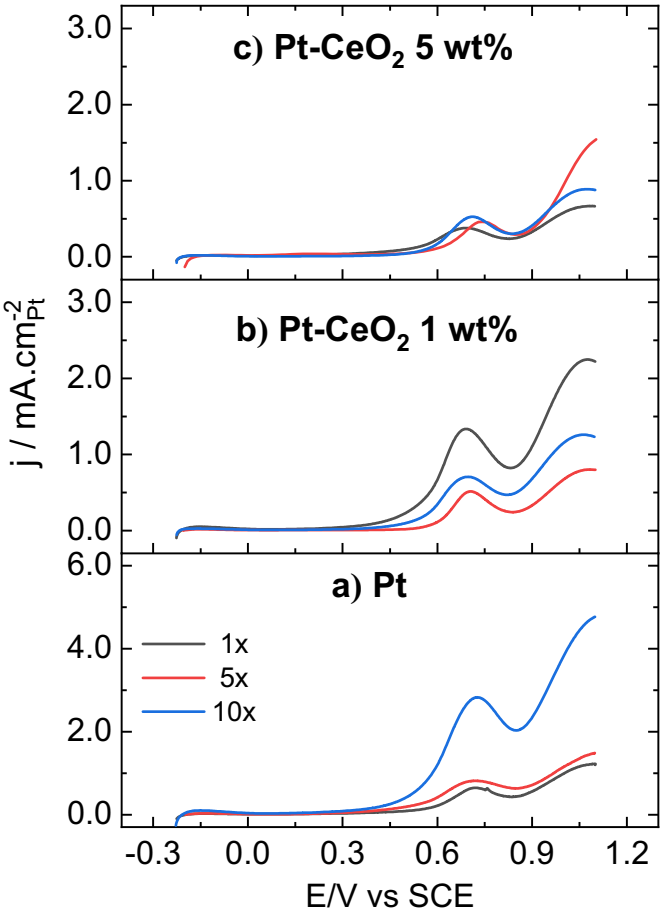

Fig. 7. Cyclic voltammograms recorded in 1 M ethanol in 0.5 M H_2SO_4 electrolyte at 50 $mV{\cdot}s^{-1}$ for (a) Pt, (b) Pt-CeO_2 1 wt% and (c) Pt-CeO_2 5 wt% composites prepared from 1× (black), 5× (red) and 10× (blue) dilution in the precursor polyester gel. The current is normalized to Pt's electrochemical surface area.

$$\%Ce(III) = \frac{Ce(III)}{Ce(III) + Ce(IV)} \times 100 = \frac{u1' + u1}{u_1' + u_1 + v_0 + v_1 + v_2 + v_0' + v_1' + v_2'} \times 100 \quad (3)$$

As shown in Fig. 5b, the %Ce (III) is lower in the Pt-CeO_2 composites (between 1 and 8%) compared to pure CeO_2 (between 10 and 15%). Also, peak v_0 is shifted to higher binding energy values in the composites with respect to pure CeO_2, Fig. 5c. As already mentioned, a strong interaction between Pt and CeO_2 explains a more positively charged cerium in the nanocomposites than in pure ceria. Interestingly, the effect of the Pt particle size (expressed in the figure as dilution of the metal precursors in the polymer precursor matrix) is more marked for the Pt-CeO_2-1 wt% catalysts.

The electrochemical characterization of the catalysts was performed by cyclic voltammetry in 0.5 M H_2SO_4. The typical cyclic voltammogram of polycrystalline Pt was recorded for all catalysts, Fig. 6. The formation of surface platinum oxides is evidenced at potentials above 0.5 V vs SCE, and their reduction in the 0.3 to 0.7 V vs SCE potential window. In the hydrogen adsorption/desorption region three peaks centered at ca. −0.13 V, ca. −0.01 V and at ca. −0.02 V vs SCE assigned to (110), (100) step and (100) terrace-flat planes [57–60], are clearly visible. The current intensity increased from pure Pt 1× to Pt 10× in accordance to the decrease of the size of the Pt NPs, as observed in Fig. 2. A similar effect, but in a lower extent is observed for the Pt-CeO_2 electrodes. In fact, the addition of ceria decreases the current intensity as the result of the coverage of the surface of the Pt NPs by the oxide, Fig. 6b and c. The electrochemical surface area (ESA) values determined from the H-desorption features of the cyclic voltammograms (CV) are reported in Table S1.

The anodic scans for the ethanol electro-oxidation reaction in H_2SO_4 electrolyte are presented in Fig. 7, and the complete cyclic voltammograms are reported in Fig. S8. The current was normalized to Pt's ESA of the corresponding catalyst. All the voltammetric features in Fig. 5 are typical of the ethanol electro-oxidation reaction catalyzed by Pt [61–63]. According to the literature, the anodic peak centered at 0.65 V vs SCE is related to the oxidation of ethanol to acetaldehyde [62]. Overall, and as expected, higher ethanol current densities were measured for catalysts with higher electrochemical surface area. As illustrated in Fig. 7, when the current is normalized to Pt's electrochemical surface area, the cyclic voltammograms of Pt 1× and Pt 5× (Fig. 7a), of Pt-CeO_2 1 wt% 5× and 10× (Fig. 5b), and of the three Pt-CeO_2 5 wt % catalysts (Fig. 7c) fairly overlap. But, interestingly, there are two singular points. First, Pt 10× shows a remarkably higher current density with respect to the Pt 1× and Pt 5×. Second, Pt-CeO_2 1 wt% — 1× shows the highest current density for the Pt-CeO_2 series. Moreover, the anodic polarization curves of these two catalysts have a pronounced shift to more negative potentials with respect to those recorded for the other catalysts (Fig. S8). For example, the potential necessary to reach 0.1 mA cm_{Pt}^{-2} is 0.320 V vs SCE for Pt 10× and 0.414 V vs SCE for Pt 5×. In the case of Pt-CeO_2 1 wt% 1× the potential is 0.410 V vs SCE which is 114 mV more negative than the value obtained with Pt 1× (0.524 V vs SCE).

The performance of the catalysts towards ethanol oxidation was also

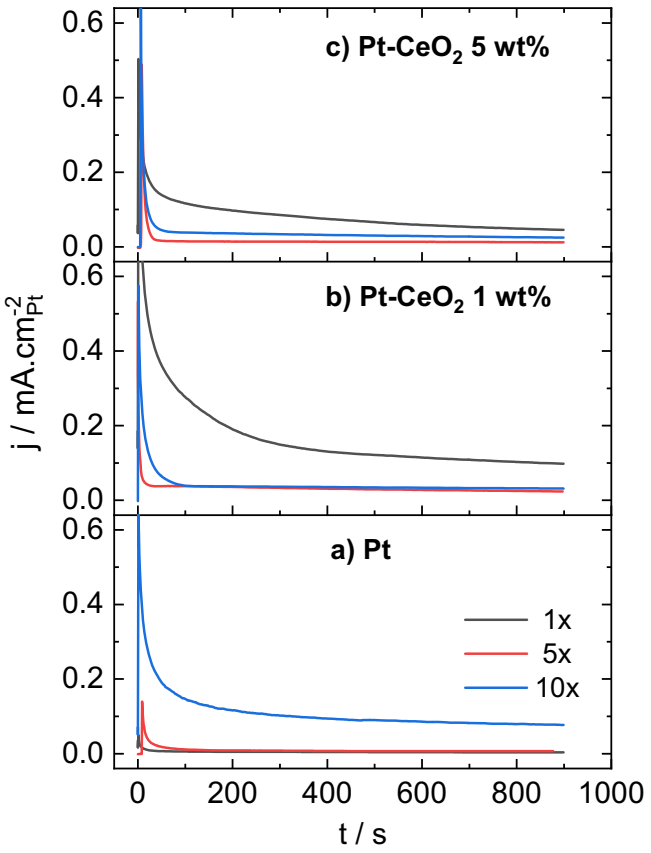

Fig. 8. Chronoamperometric measurements recorded at 0.6 V vs SCE in 1 M ethanol in 0.5 M H_2SO_4 electrolyte for (a) pure Pt, (b) Pt-CeO_2 1 wt% and (c) Pt-CeO_2 5 wt% composites prepared from 1×, 5× and 10× dilution in the precursor polyester gel. The current is normalized to Pt's electrochemical surface area.

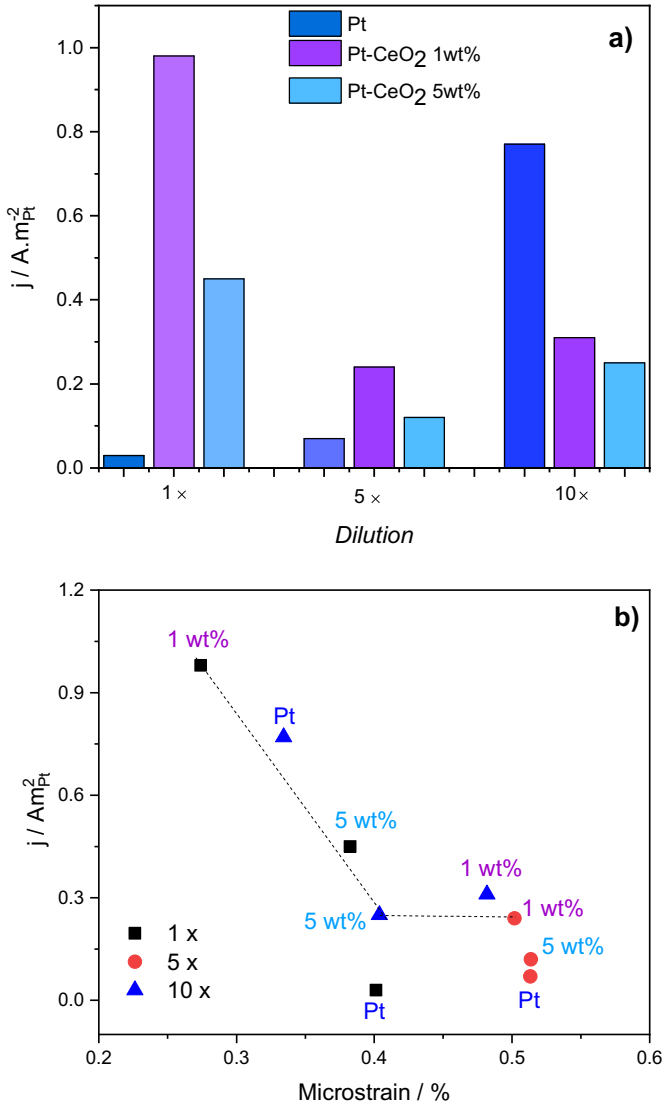

Fig. 9. (a) Current density normalized to the Pt's electrochemical surface area for the Pt, Pt-CeO_2 1 and 5 wt% composites prepared from 1×, 5× and 10× dilution in the precursor polyester gel. (b) Correlation between the current density and Pt's microstrain. The current values were taken at the end (t = 900 s) of the chronoamperometric measurements recorded at 0.6 V vs SCE in 1 M ethanol in 0.5 M H_2SO_4.

investigated in steady state conditions by chronoamperometry, Fig. 8. The currents at 900 s normalized to Pt's electrochemical surface area are shown in Fig. 9a. For the 1× series catalysts, the current density increased substantially with the addition of ceria to Pt. This increase corresponds to ~20 times for Pt-CeO_2 1 wt% and to ~10 times Pt-CeO_2 5 wt% compared to bare Pt. For the 5× series a different trend was observed, the current increased 3 times upon the addition of 1 wt% of ceria to Pt and 2 times with the addition of 5 wt% of ceria to Pt. Finally, for the 10× dilution a different trend was observed and pure Pt shows the highest catalytic activity towards the ethanol oxidation; in fact, the addition of ceria decreases the current density of about 2 times for Pt-CeO_2 1 wt% and to 3 times for Pt-CeO_2 5 wt%. Still, Pt-CeO_2 1 wt% always shows a higher current density than that of Pt-CeO_2 5 wt%. Moreover, comparing Pt 10× and Pt-CeO_2 1 wt% 1× which are composed of Pt NPs of similar size, the electrocatalytic activity of the later at t = 900 s is 1.3 times higher than that of the former. Differences in the size and agglomeration of the Pt NPs, and the absence of carbon support can justify the lower current densities observed in this work compared to those reported in the literature. The size of these Pt NPs is well above 3 nm, the optimal Pt particle size for ethanol oxidation [64,65], and above the size of the Pt NPs in the Pt/CeO_2/C composite catalysts discussed in the Introduction section (typically 5 nm) [15,16,22,23].

According to these results, few wt% of CeO_2 are sufficient to enhance the electrocatalytic activity of Pt NPs for ethanol oxidation. However, this enhancement is more meaningful on samples containing Pt NPs with large particle sizes (e.g. 20 nm as in Pt-CeO_2 1 wt% 1×). To understand why, the current density at 900 s was correlated with microstrain as shown in Fig. 9b. The catalysts with the highest activity (Pt-CeO_2 1 wt% 1×, Pt 10× and Pt-CeO_2 5 wt% 1×) are those with the microstrain below 0.36%, with the activity decreasing with increasing strain. Above 0.36% the activity does not vary significantly with the microstrain but is higher for the composites than for pure Pt. Increase of the lattice compressive strain has been related to a down-shift of the position of Pt's d-band center with respect to the Fermi level [66,67]. According to Norskov et al. [68] when the *d*-band center is shifted downwards in the energy scale, the adsorbate-metal interaction is weaker. Thus, the trend reported in Fig. 9b can be understood in terms of a negative impact of a high microstrain on the reactivity of the ethanol molecule on Pt's surface. A similar effect was previously reported on the early stages of electro-oxidation of ethanol on Pt/Sn catalysts [47] and of formic acid on Pt/Ru nanoparticle catalysts [67]. According to Fig. 3, the most active catalysts, located on the left side of Fig. 9b, are those with average particle size between 10 and 20 nm.

Fig. 9 proposes in addition that these few wt% of CeO_2 could be beneficial for the removal of CO_{ads}-like species that poison the surface of Pt. According to the XPS analysis, the addition of very small amounts of CeO_2 to Pt resulted in negative shifts of Pt's binding energy and a

more oxidized CeO_2 than in pure CeO_2. These observations suggest a weaker interaction between Pt and CO_{ads}-like species and emphasize the role of Ce^{4+} ions in the oxidative removal of these poisoning species according to Eq. (1). As previously reported by Anderson et al. [15] the more oxidized is CeO_2 (higher Ce^{4+}/Ce^{3+} ratio), the higher the catalytic activity of Pt for both methanol and ethanol oxidation in acid medium.

4. Conclusions

Pt NPs without and modified by CeO_2 (1 and 5 wt% with respect to Pt) and with average Pt particle sizes ranging from 40 nm down to 4 nm, were prepared by the Pechini method and their electrocatalytic activity for ethanol electro-oxidation in acid medium investigated. Overall, the decrease of Pt's average particle size is accompanied by an increase of the microstrain. The catalysts with the highest activity were those formed by Pt nanoparticles with average sizes between 10 and 20 nm. In particular, it was found that 1 wt% of CeO_2 can remarkably enhance the activity of 20 nm Pt NPs. This enhancement was correlated to a lower microstrain of this catalyst with respect to pure Pt, and explained in terms of a more favorable reactivity of the ethanol molecule on Pt's surface. This was also explained in terms of a strong electronic interaction between Pt and CeO_2 as shown by XPS analysis. The addition of very small amounts of CeO_2 to Pt resulted in negative shift of Pt's binding energy and a more oxidized CeO_2. These imply, respectively, a weaker interaction between Pt and CO_{ads}-like species and put in evidence the importance of Ce^{4+} ions in the oxidative removal of these poisoning species.

Acknowledgements

The authors acknowledge the financial support from NSERC Canada (Discovery grant program) and from Brazilian agencies, FAPESP (grant# 2013/0792-6), CNPq (grant# 427161/2016-9) and CAPES (code 001).

Appendix A. Supplementary data

Supplementary data to this article can be found online at https://doi.org/10.1016/j.jelechem.2019.04.008.

References

[1] Z. Zakaria, S.K. Kamarudin, S.N. Timmiati, Membranes for direct ethanol fuel cells: an overview, Appl. Energy 163 (2016) 334–342.
[2] G.L. Soloveichik, Liquid fuel cells, Beilstein J. Nanotechnol. 5 (2014) 1399.
[3] S.P.S. Badwal, S. Giddey, A. Kulkarni, J. Goel, S. Basu, Direct ethanol fuel cells for transport and stationary applications — a comprehensive review, Appl. Energy 145 (2015) 80–103.
[4] C. Lamy, E.M. Belgsir, J.-M. Léger, Electrocatalytic oxidation of aliphatic alcohols: application to the direct alcohol fuel cell (DAFC), J. Appl. Electrochem. 31 (7) (2001) 799–809.
[5] T. Iwasita, E. Pastor, A DEMS and FTIR spectroscopic investigation of adsorbed ethanol on polycrystalline platinum, Electrochim. Acta 39 (4) (1994) 531–537.
[6] J. Friedl, U. Stimming, Model catalyst studies on hydrogen and ethanol oxidation for fuel cells, Electrochim. Acta 101 (2013) 41–58.
[7] C. Xu, R. Zeng, P.K. Shen, Z. Wei, Synergistic effect of CeO_2 modified Pt/C catalysts on the alcohols oxidation, Electrochim. Acta 51 (6) (2005) 1031–1035.
[8] S. Ye, CO-tolerant catalysts, in: J. Zhang (Ed.), PEM Fuel Cell Electrocatalysts and Catalyst Layers, Springer, London, 2008, pp. 759–834.
[9] G.A. Camara, R.B. de Lima, T. Iwasita, Catalysis of ethanol electrooxidation by PtRu: the influence of catalyst composition, Electrochem. Commun. 6 (8) (2004) 812–815.
[10] M.W.A.S. Motoo, Electrocatalysis by ad-atoms — part I. Enhancement of the oxidation of methanol on platinum and palladium by gold ad-atoms, J. Electroanal. Chem. Interfacial Electrochem. 60 (1975) 259–266.
[11] M.W.A.S. Motoo, Electrocatalysis by ad-atoms. Part II. Enhancement of the oxidation of methanol on platinum by ruthenium ad-atoms, J. Electroanal. Chem. Interfacial Electrochem. 60 (1975) 267–273.
[12] D.-Y. Zhang, Z.-F. Ma, G. Wang, K. Konstantinov, X. Yuan, H.-K. Liu, Electro-oxidation of ethanol on Pt-WO_3/C electrocatalyst, Electrochem. Solid-State Lett. 9 (9) (2006) A423–A426.
[13] Y. Bai, J. Wu, J. Xi, J. Wang, W. Zhu, L. Chen, X. Qiu, Electrochemical oxidation of ethanol on Pt–ZrO_2/C catalyst, Electrochem. Commun. 7 (11) (2005) 1087–1090.
[14] X. He, C. Hu, Building three-dimensional Pt catalysts on TiO_2 nanorod arrays for effective ethanol electrooxidation, J. Power Sources 196 (6) (2011) 3119–3123.
[15] J.M. Anderson, J. Patel, A.S. Karakoti, N. Greeneltch, D.J. Díaz, S. Seal, Aging effects of nanoscale ceria in ceria–platinum composite electrodes for direct alcohol electro-oxidation, Electrochim. Acta 56 (5) (2011) 2541–2545.
[16] L. Yu, J. Xi, CeO_2 nanoparticles improved Pt-based catalysts for direct alcohol fuel cells, Int. J. Hydrog. Energy 37 (21) (2012) 15938–15947.
[17] A. Ostroverkh, V. Johánek, P. Kúš, R. Šedivá, V. Matolín, Efficient ceria–platinum inverse catalyst for partial oxidation of methanol, Langmuir 32 (25) (2016) 6297–6309.
[18] A. Trovarelli, Catalysis by Ceria and Related Materials, Imperial College Press, 2002.
[19] C. Hardacre, R.M. Ormerod, R.M. Lambert, Platinum-promoted catalysis by ceria: a study of carbon monoxide oxidation over Pt(111)/CeO_2, J. Phys. Chem. 98 (42) (1994) 10901–10905.
[20] D.-M. Gu, Y.-Y. Chu, Z.-B. Wang, Z.-Z. Jiang, G.-P. Yin, Y. Liu, Methanol oxidation on Pt/CeO_2–C electrocatalyst prepared by microwave-assisted ethylene glycol process, Appl. Catal. B Environ. 102 (1–2) (2011) 9–18.
[21] M.A. Scibioh, S.-K. Kim, E.A. Cho, T.-H. Lim, S.-A. Hong, H.Y. Ha, Pt-CeO_2/C anode catalyst for direct methanol fuel cells, Appl. Catal. B Environ. 84 (3–4) (2008) 773–782.
[22] R.F.B. De Souza, A.E.A. Flausino, D.C. Rascio, R.T.S. Oliveira, E.T. Neto, M.L. Calegaro, M.C. Santos, Ethanol oxidation reaction on PtCeO_2/C electrocatalysts prepared by the polymeric precursor method, Appl. Catal. B Environ. 91 (1–2) (2009) 516–523.
[23] D. Díaz, N. Greenletch, A. Solanki, A. Karakoti, S. Seal, Novel nanoscale ceria–platinum composite electrodes for direct alcohol electro-oxidation, Catal. Lett. 119 (3–4) (2007) 319–326.
[24] Y. Yang, Z. Zhang, Z. Hu, Activity improvement of Pt/C catalysts by adding CeO_2 nanoparticles, J. Rare Earths 29 (1) (2011) 58–63.
[25] C. Xu, P.K. Shen, Novel Pt/CeO_2/C catalysts for electrooxidation of alcohols in alkaline media, Chem. Commun. (19) (2004) 2238–2239.
[26] F. Zhang, P. Wang, J. Koberstein, S. Khalid, S.-W. Chan, Cerium oxidation state in ceria nanoparticles studied with X-ray photoelectron spectroscopy and absorption near edge spectroscopy, Surf. Sci. 563 (1–3) (2004) 74–82.
[27] A. Gupta, S. Das, C.J. Neal, S. Seal, Controlling the surface chemistry of cerium oxide nanoparticles for biological applications, J. Mater. Chem. B 4 (19) (2016) 3195–3202.
[28] D.-H. Lim, W.-D. Lee, D.-H. Choi, H.-H. Kwon, H.-I. Lee, The effect of cerium oxide nanoparticles on a Pt/C electrocatalyst synthesized by a continuous two-step process for low-temperature fuel cell, Electrochem. Commun. 10 (4) (2008) 592–596.
[29] G.-M. Schwab, Electronics of supported catalysts, in: H.P.D.D. Eley, B.W. Paul (Eds.), Advances in Catalysis, Academic Press, 1979, pp. 1–22.
[30] P.M. Pechini, Method of preparing lead and alkaline earth titanates and niobates and coating method using the same to form a capacitor, Google Patents, 1967.
[31] R.G. Freitas, R.T.S. Oliveira, M.C. Santos, L.O.S. Bulhões, E.C. Pereira, Preparation of Pt thin film electrodes using the Pechini method, Mater. Lett. 60 (15) (2006) 1906–1910.
[32] M. Kakihana, Invited review "sol-gel" preparation of high temperature superconducting oxides, J. Sol-Gel Sci. Technol. 6 (1) (1996) 7–55.
[33] H.M. Rietveld, A profile refinement method for nuclear and magnetic structures, J. Appl. Crystallogr. 2 (2) (1969) 65–71.
[34] A.C. Larson, R.B. Von Dreele, GSAS, Report lAUR, (1994), pp. 86–748.
[35] B.H. Toby, EXPGUI, a graphical user interface for GSAS, J. Appl. Crystallogr. 34 (2) (2001) 210–213.
[36] P. Thompson, D. Cox, J. Hastings, Rietveld refinement of Debye–Scherrer synchrotron X-ray data from Al_2O_3, J. Appl. Crystallogr. 20 (2) (1987) 79–83.
[37] P.W. Stephens, Phenomenological model of anisotropic peak broadening in powder diffraction, J. Appl. Crystallogr. 32 (2) (1999) 281–289.
[38] W. Qi, M. Wang, Size and shape dependent lattice parameters of metallic nanoparticles, J. Nanopart. Res. 7 (1) (2005) 51–57.
[39] I. Leontyev, A. Kuriganova, N. Leontyev, L. Hennet, A. Rakhmatullin, N. Smirnova, V. Dmitriev, Size dependence of the lattice parameters of carbon supported platinum nanoparticles: X-ray diffraction analysis and theoretical considerations, RSC Adv. 4 (68) (2014) 35959–35965.
[40] R. Prasad, V.R. Bella, A Review on Diesel Soot Emission, Its Effect and Control, 2011, (2011), p. 18.
[41] Y. Nagai, T. Hirabayashi, K. Dohmae, N. Takagi, T. Minami, H. Shinjoh, S.i. Matsumoto, Sintering inhibition mechanism of platinum supported on ceria-based oxide and Pt-oxide–support interaction, J. Catal. 242 (1) (2006) 103–109.
[42] J. Criado, M. Gonzalez, C. Real, Correlation between crystallite size and microstrains in materials subjected to thermal and/or mechanical treatments, J. Mater. Sci. Lett. 5 (4) (1986) 467–469.
[43] A. Lewera, L. Timperman, A. Roguska, N. Alonso-Vante, Metal–support interactions between nanosized Pt and metal oxides (WO_3 and TiO_2) studied using X-ray photoelectron spectroscopy, J. Phys. Chem. C 115 (41) (2011) 20153–20159.
[44] X.E. Verykios, F.P. Stein, R.W. Coughlin, Metal-support interaction effects of silver catalysts during ethylene oxidation, J. Catal. 66 (1) (1980) 147–154.
[45] K.-W. Park, J.-H. Choi, B.-K. Kwon, S.-A. Lee, Y.-E. Sung, H.-Y. Ha, S.-A. Hong, H. Kim, A. Wieckowski, Chemical and electronic effects of Ni in Pt/Ni and Pt/Ru/Ni alloy nanoparticles in methanol electrooxidation, J. Phys. Chem. B 106 (8) (2002) 1869–1877.
[46] J.B. Goodenough, R. Manoharan, A. Shukla, K. Ramesh, Intraalloy electron transfer and catalyst performance: a spectroscopic and electrochemical study, Chem. Mater.

1 (4) (1989) 391–398.
[47] S. García-Rodríguez, F. Somodi, I. Borbáth, J.L. Margitfalvi, M.A. Peña, J.L.G. Fierro, S. Rojas, Controlled synthesis of Pt-Sn/C fuel cell catalysts with exclusive Sn–Pt interaction: application in CO and ethanol electrooxidation reactions, Appl. Catal. B Environ. 91 (1–2) (2009) 83–91.
[48] T.Q. Nguyen, M.C.S. Escaño, H. Nakanishi, H. Kasai, H. Maekawa, K. Osumi, K. Sato, DFT+ U study on the oxygen adsorption and dissociation on CeO_2-supported platinum cluster, Appl. Surf. Sci. 288 (2014) 244–250.
[49] S. Gatla, D. Aubert, G. Agostini, O. Mathon, S. Pascarelli, T. Lunkenbein, M.G. Willinger, H. Kaper, Room-temperature CO oxidation catalyst: low-temperature metal–support interaction between platinum nanoparticles and nanosized ceria, ACS Catal. 6 (9) (2016) 6151–6155.
[50] R.J. Isaifan, S. Ntais, E.A. Baranova, Particle size effect on catalytic activity of carbon-supported Pt nanoparticles for complete ethylene oxidation, Appl. Catal. A Gen. 464–465 (2013) 87–94.
[51] J. Radnik, C. Mohr, P. Claus, On the origin of binding energy shifts of core levels of supported gold nanoparticles and dependence of pretreatment and material synthesis, Phys. Chem. Chem. Phys. 5 (1) (2003) 172–177.
[52] P.S. Bagus, C.J. Nelin, E. Kay, F. Parmigiani, Reply to the comment by DiCenzo and Wertheim on “core binding energies for clusters···”, J. Electron Spectrosc. Relat. Phenom. 43 (3) (1987) C13–C18.
[53] P. Claus, A. Brückner, C. Mohr, H. Hofmeister, Supported gold nanoparticles from quantum dot to mesoscopic size scale: effect of electronic and structural properties on catalytic hydrogenation of conjugated functional groups, J. Am. Chem. Soc. 122 (46) (2000) 11430–11439.
[54] E. Paparazzo, G.M. Lngo, N. Zacchetti, X-ray induced reduction effects at CeO_2 surfaces: an X-ray photoelectron spectroscopy study, J. Vac. Sci. Technol. A 9 (3) (1991) 1416–1420.
[55] I. Avramova, S. Suzer, D. Guergova, D. Stoychev, P. Stefanov, CeO_x/Al_2O_3 thin films on stainless steel substrate — dynamical X-ray photoelectron spectroscopy investigations, Thin Solid Films 536 (2013) 63–67.
[56] J.F. Moulder, W.F. Sickle, P.E. Sobol, K.D. Bomben, Handbook of X-ray Photoelectron Spectroscopy: A Reference Book of Standard Spectra for Identification and Interpretation of XPS Data, Physical Electronics Division, Perkin-Elmer Corporation, 1992.
[57] N.M. Markovic, H.A. Gasteiger, P.N. Ross, Oxygen reduction on platinum low-index single-crystal surfaces in sulfuric acid solution: rotating ring-Pt(hkl) disk studies, J. Phys. Chem. 99 (11) (1995) 3411–3415.
[58] G.A. Attard, J.E. Gillies, C.A. Harris, D.J. Jenkins, P. Johnston, M.A. Price, D.J. Watson, P.B. Wells, Electrochemical evaluation of the morphology and enantioselectivity of Pt/graphite, Appl. Catal. A Gen. 222 (1–2) (2001) 393–405.
[59] R. Gómez, J. Clavilier, Electrochemical behaviour of platinum surfaces containing (110) sites and the problem of the third oxidation peak, J. Electroanal. Chem. 354 (1–2) (1993) 189–208.
[60] A. Ponrouch, S. Garbarino, E. Bertin, C. Andrei, G.A. Botton, D. Guay, Highly porous and preferentially oriented {100} platinum nanowires and thin films, Adv. Funct. Mater. 22 (19) (2012) 4172–4181.
[61] H. Wang, Z. Jusys, R.J. Behm, Ethanol and acetaldehyde adsorption on a carbon-supported Pt catalyst: a comparative DEMS study, Fuel Cells 4 (1–2) (2004) 113–125.
[62] A.A. Abd-El-Latif, E. Mostafa, S. Huxter, G. Attard, H. Baltruschat, Electrooxidation of ethanol at polycrystalline and platinum stepped single crystals: a study by differential electrochemical mass spectrometry, Electrochim. Acta 55 (27) (2010) 7951–7960.
[63] R.B. Moghaddam, P.G. Pickup, Support effects on the oxidation of ethanol at Pt nanoparticles, Electrochim. Acta 65 (0) (2012) 210–215.
[64] J. Perez, V.A. Paganin, E. Antolini, Particle size effect for ethanol electro-oxidation on Pt/C catalysts in half-cell and in a single direct ethanol fuel cell, J. Electroanal. Chem. 654 (1) (2011) 108–115.
[65] P.G. Corradini, N.A. Santos, G.C. Silva, J. Perez, Pt–rare earth catalysts for ethanol electrooxidation: modification of polyol synthesis, J. Solid State Electrochem. 20 (9) (2016) 2581–2587.
[66] Y. Shen, M.Z. Zhang, K. Xiao, J. Xi, Synthesis of Pt, PtRh, and PtRhNi alloys supported by pristine graphene nanosheets for ethanol electrooxidation, ChemCatChem 6 (11) (2014) 3254–3261.
[67] M.A. Rigsby, W.-P. Zhou, A. Lewera, H.T. Duong, P.S. Bagus, W. Jaegermann, R. Hunger, A. Wieckowski, Experiment and theory of fuel cell catalysis: methanol and formic acid decomposition on nanoparticle Pt/Ru, J. Phys. Chem. C 112 (39) (2008) 15595–15601.
[68] B. Hammer, J.K. Norskov, Electronic factors determining the reactivity, Surf. Sci. 343 (1995) 211–220.